


Summer 2022

The significance of cell-surface α 2,3-linked Sialic Acid in Osteoclasts

Christopher S. Harding

Follow this and additional works at: <https://dc.ewu.edu/theses>

 Part of the [Genetic Phenomena Commons](#), [Genetic Structures Commons](#), [Medical Genetics Commons](#), and the [Musculoskeletal Diseases Commons](#)

THE SIGNIFICANCE OF CELL-SURFACE α 2,3-LINKED SIALIC ACID IN
OSTEOCLASTS

A Thesis

Presented To

Eastern Washington University

Cheney, Washington

In Partial Fulfillment of the Requirements

for the Degree


Master of Science in Biology

By

Christopher S. Harding

Summer 2022

THESIS OF CHRISTOPHER S. HARDING APPROVED BY

 _____ DATE 10-05-2022

DR. JASON W. ASHLEY, PhD – CHAIR, GRADUATE STUDY
COMMITTEE

 _____ DATE 10/05/2022

DR. ANDREA CASTILLO, PhD – MEMBER, GRADUATE STUDY
COMMITTEE

 _____ DATE 10-5-22

DR. ERIC ABBEY, PhD – MEMBER, GRADUATE STUDY
COMMITTEE

ABSTRACT

THE SIGNIFICANCE OF CELL-SURFACE α 2,3-LINKED SIALIC ACID IN
OSTEOCLASTS

By

Christopher S. Harding

Summer 2022

Osteoclasts are giant, multinucleated cells that, alongside osteoblasts, are central to maintaining physiologically healthy bone. The functions of osteoclasts and osteoblasts—degrading and depositing bone matrix, respectively—are paired in healthy bone tissue, thereby yielding no net bone loss or deposition. When these functions become imbalanced, it results in net bone loss or gain, depending on which cell type is being outcompeted. Osteoporosis is one of the most common pathologies stemming from such an imbalance, and predominantly affects postmenopausal women, as the ablation of circulating estrogen—a pro-death signal for osteoclasts—causes a prolongation of osteoclast lifespan and consequent lengthening of their resorptive activity. This results in a net bone loss and fragile bones, which poses a serious health risk to the affected individuals. Novel methods for inhibiting the

formation or function of osteoclasts are of clinical significance, as many current therapies are either cost-prohibitive for some, or the therapy can only be supplied for so long before adverse effects from the therapy start taking a toll. In this study we sought to determine the effect that α 2,3-linked sialic acid on the surface of osteoclast precursors has on the formation or function of mature osteoclasts. Previous work by our lab lead, Dr. Jason W. Ashley, initially showed that a prevalent osteoclast biomarker, CD68, is heavily glycosylated during osteoclastogenesis, and further work by previous graduate students indicated that removal of α 2,3-linked sialic acid adversely affected the formation of mature osteoclasts. We were able to verify that there is widespread α 2,3-sialylation of osteoclasts during their differentiation, however, we were unable to reproduce—in RAW 264.7 cells—the morphological changes previously seen in primary bone marrow macrophages following cell-surface α 2,3-linked sialic acid ablation. Due to inherent variation between replicate experiments arising from the use of RAW 264.7 cells, this phenomenon could not be validated statistically.

ACKNOWLEDGEMENTS

Undergraduate Research Assistants:

Katheryn Collins (current graduate student in L. Matos lab), for her assistance with various troubleshooting experiments early on.

Lorren Morgan, for his assistance with various intermediate experiments.

Eastern Washington University Faculty and Staff:

Dr. Jason W. Ashley, Department of Biology, thesis advisor.

Dr. Andrea Castillo, Department of Biology, internal committee member.

Dr. Eric Abbey, Department of Chemistry, external committee member.

Dr. Nicolas Burgis, Department of Chemistry, for his advice and assistance in recombinant protein purification.

Dr. Kriztian Magori, Department of Biology, for his assistance with statistics and data analysis.

Richard Barido, Vivarium, for his general assistance with numerous odds and ends, especially during the pandemic.

INTRODUCTION

Osteoporosis is a prevalent disease among older adults, with major associated health risks. It has been previously extrapolated that, as of this year, approximately 11.9 million adults 50 years or older have osteoporosis, and approximately 52 million adults in the same age group have low bone mass in general. By 2030 those numbers are projected to be 13.2 million and 57.4 million, respectively (Wright et al., 2014). In diseases such as rheumatoid arthritis and osteoporosis, the processes of osteoclastogenesis and osteoclast function are in an unbalanced and unregulated state, in which the activity of osteoclasts outpaces the activity of osteoblasts, leading to net bone loss. Furthermore, such a state can also create a more favorable environment for the metastasis of cancers to the bone. Osteoclasts are multinucleated, bone-resorbing cells that are pivotal in the physiologic process of bone remodeling and in degenerative bone-loss diseases, though they are also central to some disorders of excessive bone accumulation (Teitelbaum, 2007). The processes of osteoclast development and function are normally coupled with the activity of bone-depositing osteoblasts, creating a balanced cycle of bone removal and bone deposition.

Understanding the precise mechanisms involved in the differentiation and physiological function of osteoclasts can open avenues for the development and application of differing therapeutic

strategies to combat unregulated osteoclast development or activity. While the general mechanism of osteoclast differentiation and resorptive function is well understood, some of the more minute molecular interactions are not sufficiently characterized. One of these poorly understood interactions is the effect that the presence of α 2,3-linked sialic acid in various cell-surface molecules on osteoclasts, and their precursors, has on the formation and function of mature osteoclasts. Thus, our goal for this project was to define what effect, if any, α 2,3-linked sialic acid has on the process of osteoclastogenesis via obstruction of the gene *SIAT4A*, which encodes the information for the sialyltransferase ST3Gal, whose function it is to add sialic acid in the linkage pattern of interest.

The process of osteoclastogenesis is regulated predominantly by two cytokines: Macrophage Colony-Stimulating Factor (M-CSF) and Receptor-Activator of Nuclear Factor- κ B Ligand (RANKL) (Teitelbaum, 2007). Macrophages are first “primed” by M-CSF, which stimulates macrophage survival through the phosphoinositide 3-kinase (PI3K)/Akt and protein lipase (PLC)/Bcl-xL pathways, as well as by Fms-interacting protein (FIMP) inactivation (Stanley & Chitu, 2014). M-CSF also stimulates macrophage proliferation via the MAPK/ERK kinase (MEK)/ERK, PI3K/Akt, and c-Jun N-terminal kinase (JNK) pathways.

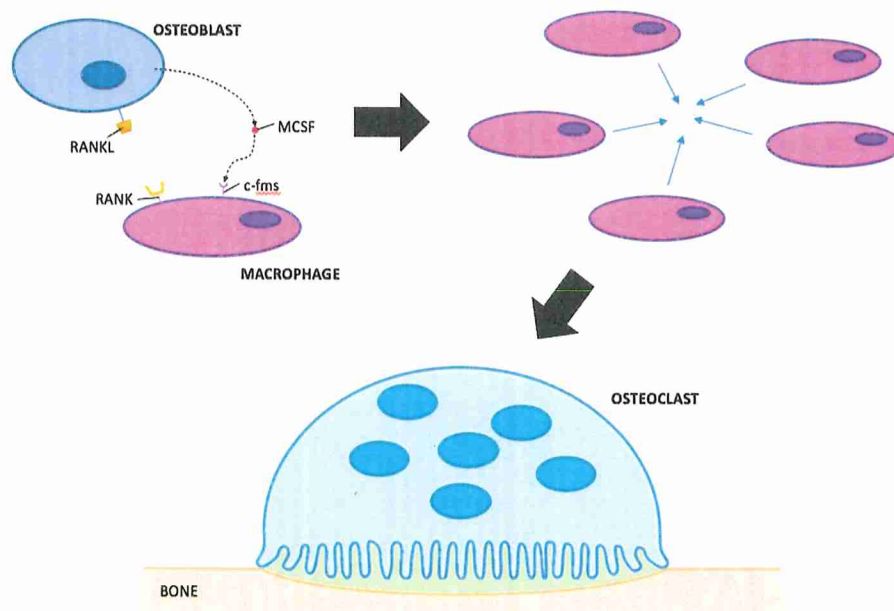


Figure 1. Osteoclastogenesis. M-CSF promotes macrophage proliferation and survival, as well as stimulates the expression of RANK on the macrophage surface. RANKL stimulates the expression of osteoclast-specific genes and drives the cell-cell fusion event between multiple macrophages to form the mature, multinucleated osteoclast.

Additionally—and critically—M-CSF promotes substantially increased expression of RANK—RANKL’s receptor—on the macrophage surface (Arai et al., 1999; Takayanagi, 2007). Subsequently, RANKL induces the differentiation process by stimulating nuclear factor kappa-B (NF- κ B), which in turn induces expression of nuclear factor of activated T-cells cytoplasmic 1 (NFATc1)—the key regulator of osteoclastogenesis (Park et al., 2017). After RANKL-stimulation the macrophages will differentiate into mononuclear osteoclasts, multiple of which will later fuse together to form multinucleated, mature osteoclasts (Fig. 1). This cell-cell fusion event is key in the formation of properly functional osteoclasts because

mononuclear osteoclasts, while still able resorb bone, do so with reduced efficiency (Takahata et al., 2007).

Glycosylation is a ubiquitous form of posttranslational modification that occurs in all cell types. The physiological effects of glycosylation are difficult to isolate, and even more difficult to predict, for reasons such as variation in glycosylation patterns between species (and sometimes even within species), the ability for the same glycan (monosaccharide moiety) to be integrated into different glycoconjugates at different stages and in different tissue types, and that a given glycosylation site can play host to several similarly structured glycans within a given species. Some general functions of glycans have been elucidated, including intrinsic recognition and extrinsic recognition, wherein glycans mediate cell-cell interactions and cell-microbe interactions, respectively. Some examples of cell-cell interaction facilitated by glycans are the recognition of endothelial cell ligand glycans by adhesion molecules of the selectin family on leukocytes, allowing the two cell types to associate when they come into contact, and the recognition of oocyte surface glycans – specifically terminal sialic acid residues – by the sperm, which triggers the release of acrosomal enzymes from the head of the sperm (acrosomal reaction) (Takahata et al., 2007).

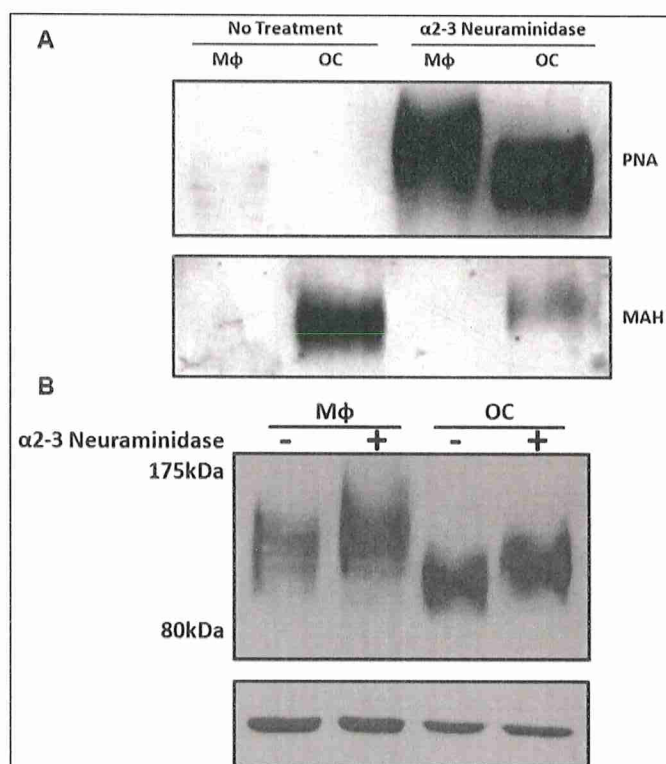


Figure 2. RANKL increases terminal sialylation of CD68. (A) Immunoprecipitated CD68 with/without α 2-3 neuraminidase digestion. PNA lectin binds to desialylated galactose moieties; MAH binds to α 2,3-linked Sia moieties. (B) Macrophage and osteoclast whole-cell lysate immunoblotted for CD68 and b-actin (loading control) with/without α 2-3 neuraminidase digestion.

In research previously done by J.W. Ashley (Ashley, 2011), it was shown that the sialylation status of CD68 – a type I transmembrane glycoprotein widely expressed on the surface of monocytes, macrophages, and osteoclasts – is upregulated in response to RANKL stimulation (Fig. 2A). As indicated in the ‘MAH’ row of the blot, α 2,3-linked cell surface sialylation is not present in macrophages, but can be seen prominently in osteoclasts, which is later largely reduced by treatment with an α 2,3 neuraminidase. In an experiment performed by Abigail Keever, a previous

graduate student in Dr. Ashley's lab, treatment of bone marrow-derived macrophages (BMMs) with $\alpha 2,3$ neuraminidase resulted in reduced size and an aberrant morphology as they matured into osteoclasts (Fig. 3) (Keever, 2019).

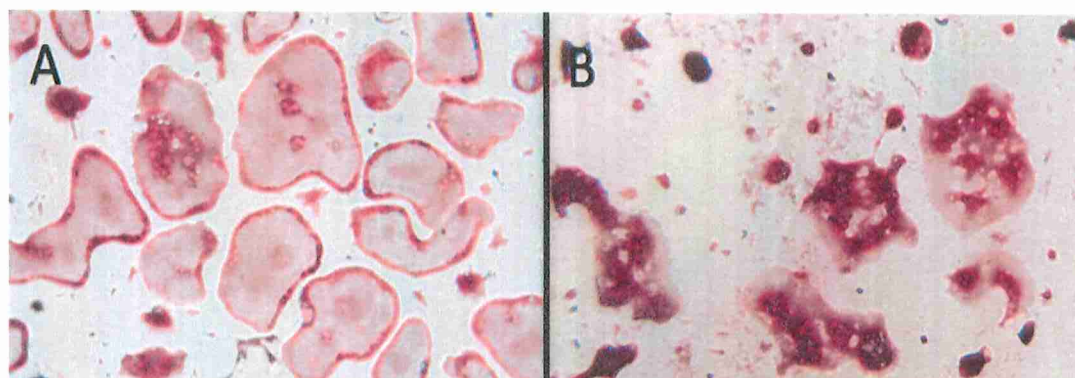


Figure 3. Terminally differentiated osteoclasts derived from BMMs with/without sialidase pre-treatment. (A) Osteoclasts resulting from macrophages treated solely with RANKL. (B) Osteoclasts resulting from macrophages treated with RANKL + $\alpha 2,3$ neuraminidase.

To ascertain whether this was truly the result of macrophage desialylation and not the result of an immunological response to the exogenous nature of the sialidase (cloned from *Streptococcus pneumoniae*) we approached the removal of cell-surface $\alpha 2,3$ -linked sialic acid (Sia) from an endogenous standpoint. We attempted to knockdown the mRNA for *SIAT4A*, the gene encoding ST3Gal1—the sialyltransferase primarily responsible for the addition of terminal $\alpha 2,3$ -linked sialic acid onto substrates containing galactose residues. The sialyltransferase ST3Gal1 is normally found in the Golgi apparatus—though it can be proteolytically cleaved into a soluble form—and catalyzes the addition of sialic acid in an $\alpha 2-3$ configuration to galactose moieties attached to

glycolipids or proteins, using cytidine monophosphate-sialic acid (CMP-Sia) as the donor substrate (Fig. 4).

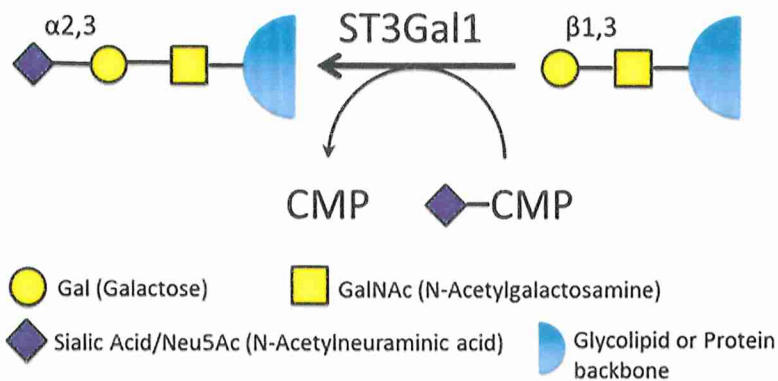


Figure 4. Addition of $\alpha 2,3$ -linked sialic acid by ST3Gal1. ST3Gal1 is normally found in the Golgi apparatus, where it catalyzes the transfer of sialic acid from the donor molecule (CMP-Sia) onto a galactose-containing glycolipid/glycoprotein, wherein the galactose is linked in a $\beta 1,3$ pattern to an *N*-acetylgalactosamine (GalNAc).

TABLE OF CONTENTS

Chapter	Page
I. Methods.....	1
II. Results.....	10
III. Discussion.....	19
References.....	22
Vita.....	24
 Figure List	
i. Figure 1.....	viii
ii. Figure 2.....	x
iii. Figure 3.....	xi
iv. Figure 4.....	xii
v. Figure 5.....	3
vi. Figure 6.....	4
vii. Figure 7.....	10
viii. Figure 8.....	11
ix. Figure 9.....	12
x. Figure 10.....	12
xi. Figure 11.....	13
xii. Figure 12.....	14
xiii. Figure 13.....	15

xiv.	Figure 14.....	16
xv.	Figure 15.....	16
xvi.	Figure 16.....	17
xvii.	Figure 17.....	18
xviii.	Figure 18.....	19

Table List

i.	Table 1.....	5
ii.	Table 2.....	6
iii.	Table 3.....	6

METHODS

Differentiation of RAW 264.7 cells

RAW 264.7 murine macrophage cells (ATCC, TIB-71) seeded at a density of 50,000 cells/mL were treated with 100 ng/mL of RANKL for 96 hours to stimulate differentiation into osteoclasts. Medium (DMEM, 10% heat-inactivated FBS, 1% glutamine, 1% non-essential amino acids) containing RANKL was refreshed after 48 hours to replenish nutrients and maintain differentiation signal. Volumes seeded depended on culture vessel—200 μ L/well in a 96-well plate, 1 mL/well in a 24-well, 4 mL in a 60 mm dish, and 10 mL in a 10 cm dish.

Direct delivery of siRNAs

Three different predesigned Dicer-Substrate small interfering RNA (siRNA) (DsiRNA) mouse gene sequences were obtained from IDT as part of a TriFECTa DsiRNA Kit (Design ID: mm.Ri.St3gal1.13). Transfection of RAW 264.7 cells in a 96-well plate 24 or 48 hours post RANKL-stimulation was accomplished using Lipofectamine RNAiMAX (Invitrogen, 13778) and following the product's transfection protocol. We amended the amount of siRNA used per well to be ten-fold higher (100nM/well) than what was listed in the protocol to match the concentration that Li et al. (2015) found yielded the greatest level of inhibition in RAW 264.7 cells.

Cloning and viral delivery of shRNAs

Oligonucleotides encoding short hairpin RNA (shRNA) molecules were generated using the siRNA/shRNA/Oligo Optimal Design web tool designed by the Kay Lab at Stanford Medicine (<https://web.stanford.edu/group/markkaylab/cgi-bin/>) and cloned into a modified ecotropic—mouse- and rat-specific—retroviral pMXs-Puro plasmid (Cell BioLabs, VPK-300) (Fig. 5). The retroviral packaging cell line Platinum-E (Plat-E) cells (Cell Biolabs Inc, RV-101) were subsequently transfected with the recombinant pMXs plasmids and the VSV-G envelope-expressing plasmid pMD2.G (Addgene, 12259) (Fig. 6)—to facilitate increased viral particle transfection—using FuGENE HD Transfection Reagent (Promega, E2311) following the manufacturer protocol. Virally-conditioned medium from propagating Plat-E cells was collected, filtered through a 0.45- μ m syringe filter, combined with Polybrene Infection/Transfection Reagent (8 μ g/mL; Sigma-Aldrich, TR-1003), and used to inoculate RAW 264.7 cells. Transduced RAW 264.7 cells were allowed to grow for 48 hours, after which the medium was refreshed with 2 μ g/mL puromycin-supplemented medium to select for the recombinant retroviral plasmid.

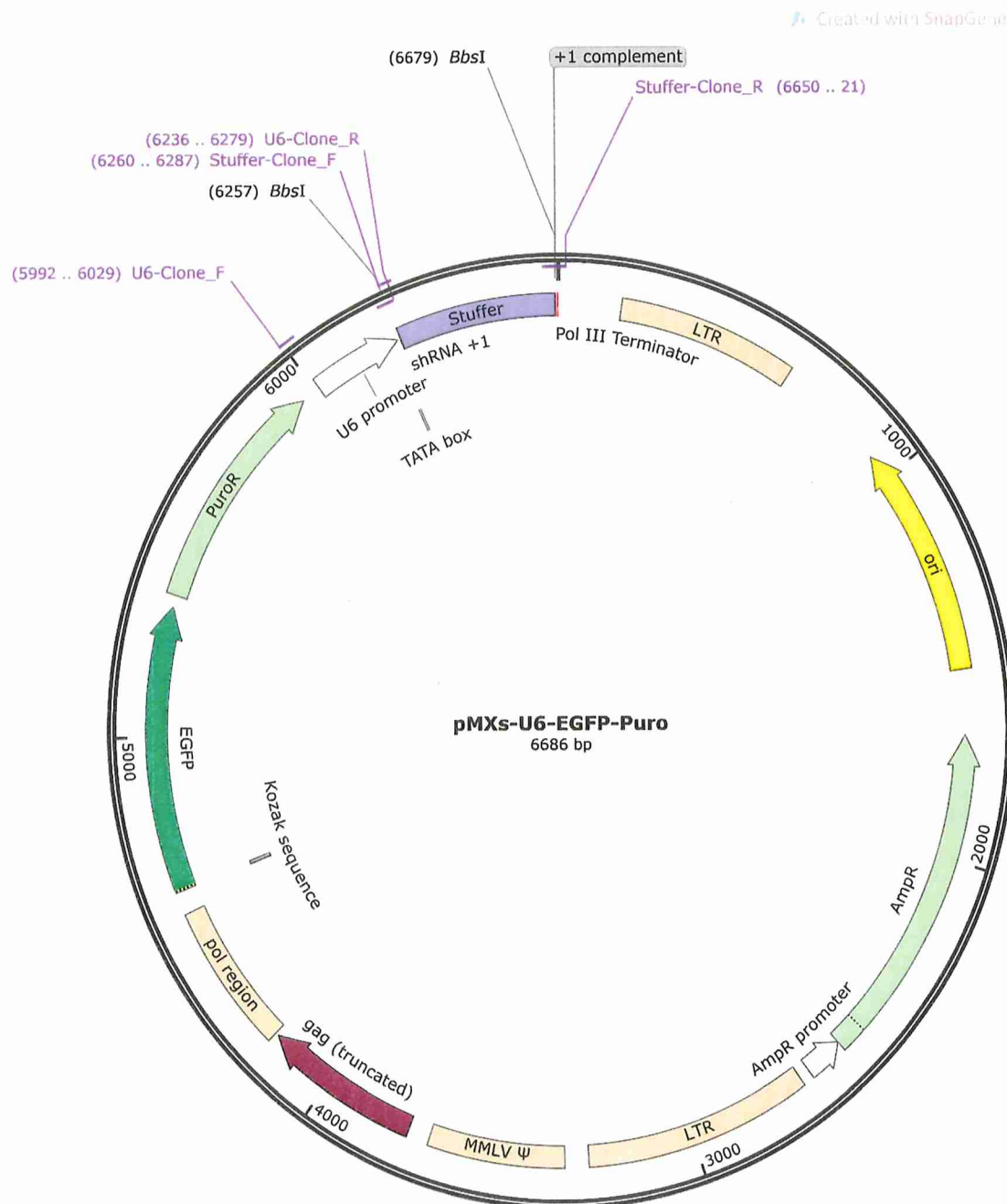


Figure 5. Map of modified ecotropic pMXs plasmid. The restriction enzyme BbsI was used to open this plasmid, releasing the “Stuffer” sequence. Predesigned double-stranded shRNA sequences were subsequently inserted into that space and ligated together during PCR amplification.

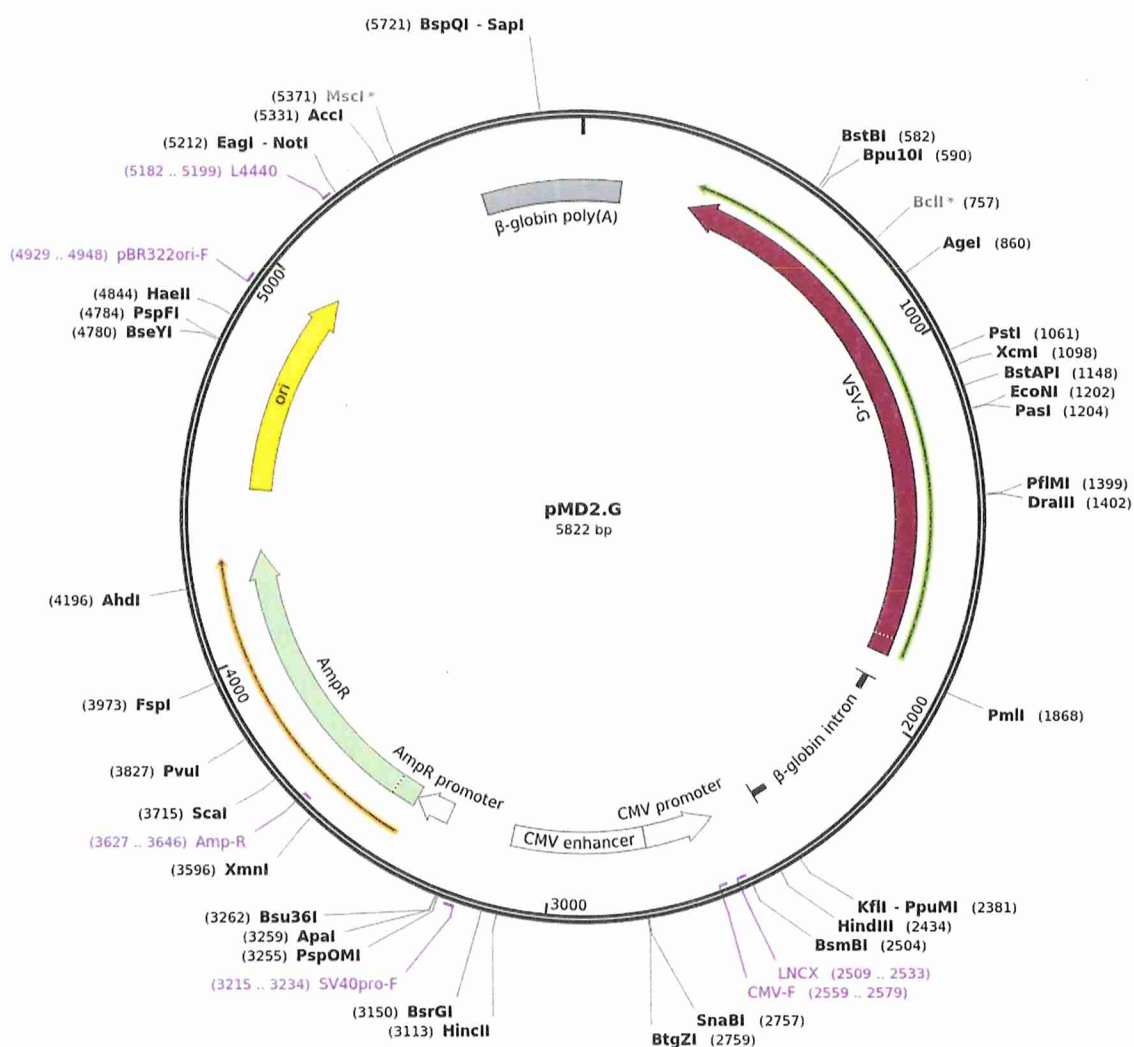


Figure 6. Map for plasmid encoding pantropic viral envelope protein VSV-G.

α 2-3 Neuraminidase Treatment

Initially, RAW 264.7 cells were seeded in a 96-well plate (50,000 cells/mL), stimulated with RANKL, and allowed to incubate for 48 hours to ensure the cells were committed to becoming osteoclasts. α 2-3 Neuraminidase S from New England BioLabs (P0743) was added at a concentration of 25 units/mL per well of committed cells and incubated

at 37°C for 1 hour. In addition to native α 2-3 Neuraminidase S, other subsets of RANKL-stimulated cells were treated with α 2-3 Neuraminidase S that had been heat-inactivated at 75°C for 10 minutes to control for the exogenous nature of the protein, and with PBS as a manipulation control.

Quantification of gene expression via quantitative real-time polymerase chain reaction (RT-qPCR)

RNA was isolated from cells using Zymogen's Quick RNA Microprep Kit (R1050/R1051), following the manufacturer's protocol. RT-qPCR was performed using predesigned PrimeTime qPCR probe assays from Integrated DNA Technologies (IDT; B2M - Mm.PT.39a.22214835, SIAT4A - Mm.PT.58.16698772, NFATc1 - Mm.PT.58.7040453) and the Luna Universal Probe One-Step RT-qPCR Kit (New England BioLabs, E3005); the composition of the reaction is shown in Table 1, and the thermocycler parameters are shown in Table 2.

Table 1. RT-qPCR Master Mix Components

COMPONENT	20μL REACTION	FINAL CONCENTRATION
Luna Universal Probe One-Step Reaction Mix (2X)	10 μ L	1X
Luna WarmStart® RT Enzyme (20X)	1 μ L	1X
B2M PrimeTime qPCR Probe Assay (10X)	2 μ L	1X
SIAT4A PrimeTime qPCR Probe Assay (10X)	2 μ L	1X
Template RNA	5 μ L	\leq 1 μ g (total RNA)

Table 2. Thermocycler Parameters

CYCLE STEP	TEMPERATURE	TIME	CYCLES
Reverse Transcription	55°C	10 minutes	1
Initial Denaturation	95°C	1 minute	1
Denaturation	95°C	1 minute	55
Extension	60°C	30 seconds	55

Reducing SDS-PAGE

Clarified whole-cell lysates from lysed osteoclasts were run on 4-12% Bolt™ Bis-Tris gels (Invitrogen, NW04120BOX) under reducing conditions. Protein samples were prepared using 4X Bolt™ LDS Sample Buffer (Invitrogen, B0007) and β -mercaptoethanol (Table 3), loaded at 20-40 μ g/lane, and run for 30 minutes at 200V. Gels were subsequently stained for 30 minutes with 1 μ L SYPRO Tangerine (Invitrogen, S12010) in 20 mL PBS with gentle rocking, followed by three washes in PBS with vigorous rocking.

Table 3. Reducing SDS-PAGE Sample Preparation. Only 20 μ L of sample preparations were loaded per lane on a 10-well mini gel.

COMPONENT	25μL REACTION	FINAL CONCENTRATION
Protein	variable	(1 μ g/ μ L)
Bolt™ LDS Sample Buffer (4X)	6.25 μ L	1X
β -mercaptoethanol	1.25 μ L	1:20

dH₂Oto 25 μ L

NA

Western blotting

Three different anti-human ST3Gal1 antibodies were employed for protein visualization (LifeSpan BioSciences, LS-C747031-50; Novus Biologicals, NBP1-62540; ThermoFisher, PA588176). Proteins were transferred to a nitrocellulose membrane via a wet-transfer method and 1X Bolt™ Transfer Buffer (Invitrogen, BT0006) at 10V for 1 hour. Initial blocking of the membrane occurred in 5% milk/TBS-T solution for 1 hour at room temperature, followed by an overnight incubation with the primary antibody (1:1000) in 5% milk/TBS-T solution at 4°C. Subsequently, the membrane was incubated with HRP-linked secondary antibody (1:2000) in 5% milk/TBS-T solution for 1 hour at room temperature. The membrane was washed three times with 1X Tris-buffered saline, 0.1% Tween® 20 (TBS-T) for 5 minutes each with vigorous washing in between the blocking and incubation steps.

Lectin blotting

Biotinylated *Maackia amurensis* lectin II (MAL-II; Vector Labs, B-1265-1) was used to detect the presence of α 2,3-linked sialic acid on the surface of mature osteoclasts. Protein obtained from osteoclast lysis was run on a reducing SDS-PAGE and subsequently transferred to a nitrocellulose membrane. Initial blocking of the membrane occurred in

5% BSA in TBS-T overnight at 4°C. Using the VECTASTAIN® Elite® ABC-HRP Peroxidase Kit (Vector Labs, PK-6100), the membrane was blocked first with the avidin block in 0.5% BSA/TBS-T for 30 min (2 drops/10mL), then the biotin block in 0.5% BSA/TBS-T for 30 min (2 drops/10mL), with three 5 min washes in 1X TBS-T after each blocking step. The membrane was then incubated for 1 hour with the biotinylated MAL-II in 0.5% BSA/TBS-T (1µg/1mL), followed by washing in 1X TBS-T. Next, the membrane was incubated in the ABC-HRP complex (2 drops A + 2 drops B/15mL) in 0.5% BSA/TBS-T for 30 minutes, followed by washing in 1X TBS-T. Lastly, a 5-minute incubation with a 1:1 DuoLux chemiluminescent/fluorescent substrate mix for peroxidase (Vector Labs, EW-93952-08).

Fluorescent staining

Terminally differentiated osteoclasts were treated with diamidino-2-phenylindole (DAPI) and CF®488A-conjugated phalloidin (Biotium, 0042) to stain DNA and actin, respectively. A master mix of 1 µg/mL DAPI and 2.5 µL stock phalloidin-CF®448A in 100 µL PBS/well was prepared. Cells were washed initially three times with warm PBS, followed by fixation at room temperature for 15 minutes in a 10% neutral-buffered formalin solution. After fixation, cells were washed three times with PBS, permeabilized with 0.5% Triton X-100 in PBS for 10 minutes at room temperature, and then washed thrice more with PBS.

The fluorescent stain master mix was then applied and allowed to incubate for 20 minutes at room temperature. Following staining, the cells were washed a final three times with PBS, leaving the final wash in the wells for image acquisition.

RESULTS

SIAT4A Knockdown

For our siRNA work, we set a goal for 70% transfection efficiency, based upon siRNA validation screening work performed by Krueger et al. (2007). In our attempts using siRNA to ameliorate gene expression we were unable to attain transfection efficiency above 55%, even when using a greater amount of the transfection reagent to facilitate siRNA uptake, as illustrated by both fluorescent imaging (Fig. 7) and quantification (Fig. 8).

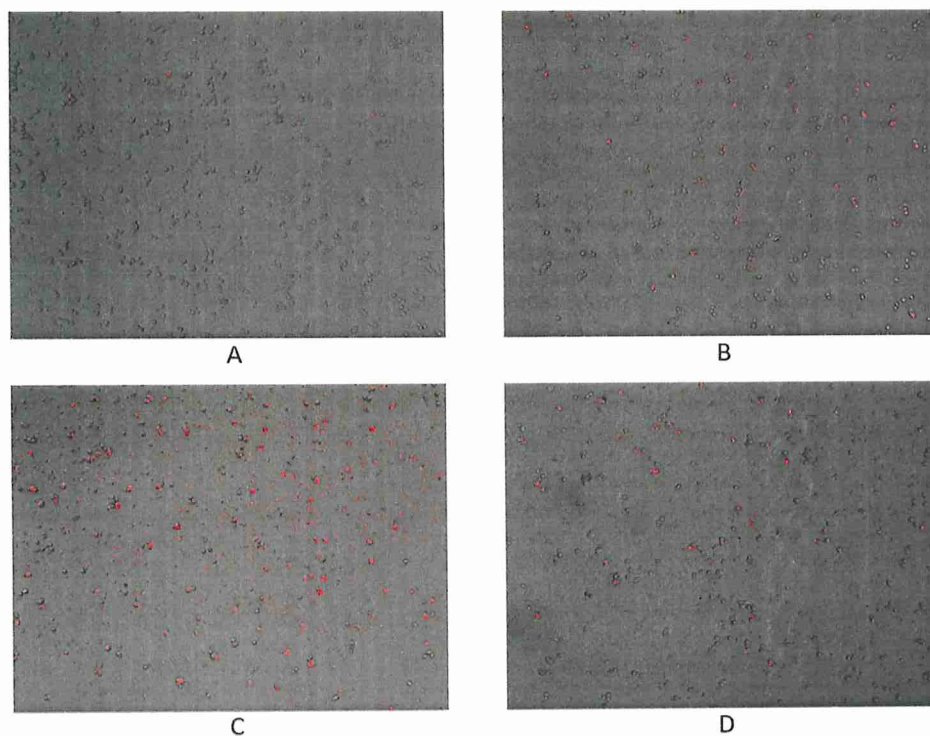


Figure 7. Comparison of Lipofectamine RNAiMAX transfection efficiency. RAW 264.7 cells were transfected with a labeled non-targeting siRNA using varying amounts of Lipofectamine reagent to visualize transfection efficiency and determine if the reagent was cytotoxic at or above a certain level. (A) 0.3 $\mu\text{L}/\text{well}$ (*protocol-recommended volume*), (B) 0.5 $\mu\text{L}/\text{well}$, (C) 0.8 $\mu\text{L}/\text{well}$, (D) 1 $\mu\text{L}/\text{well}$. Images were taken at 10X magnification.

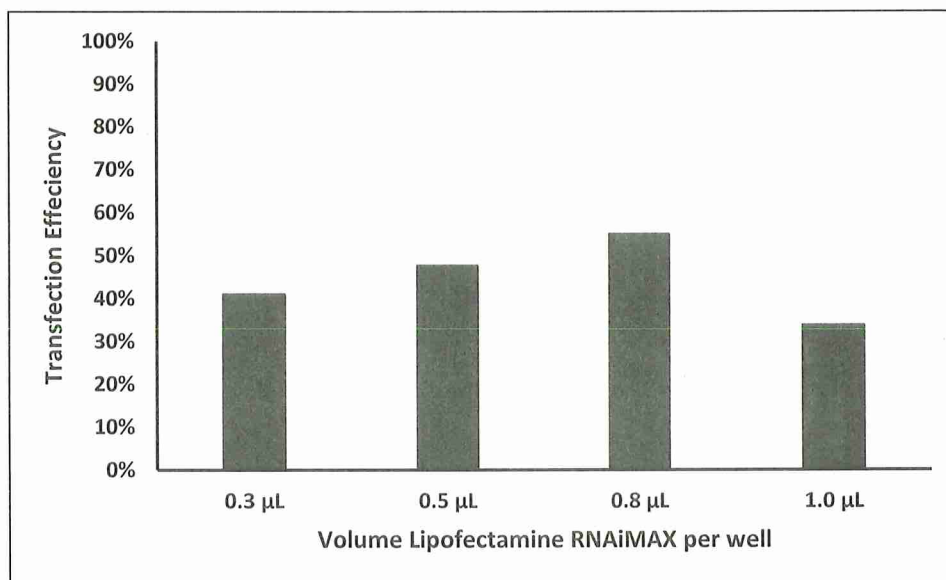


Figure 8. Quantitated siRNA Transfection Efficiency. Efficiency of siRNA delivery did not appear to notably change when using higher than the volume recommended by the manufacturer protocol (0.3μL/well). Data is representative of one experiment using only a single replicate.

RT-qPCR analysis of mRNA expression following varying siRNA concentrations verified that 100nM yielded the highest level of knockdown, as shown by Li et al. (2015) (Fig. 9). Subsequent experimentation using 100nM siRNA did not yield consistent levels of knockdown. One variant (siRNA-1) was ruled out due to inexplicably—and paradoxically—high relative *SIAT4A* expression following treatment, while the other two siRNA variants yielded a mean reduction of 17% and 20% in macrophages, and a 24% and 25% mean reduction in osteoclasts, respectively (Fig. 10).

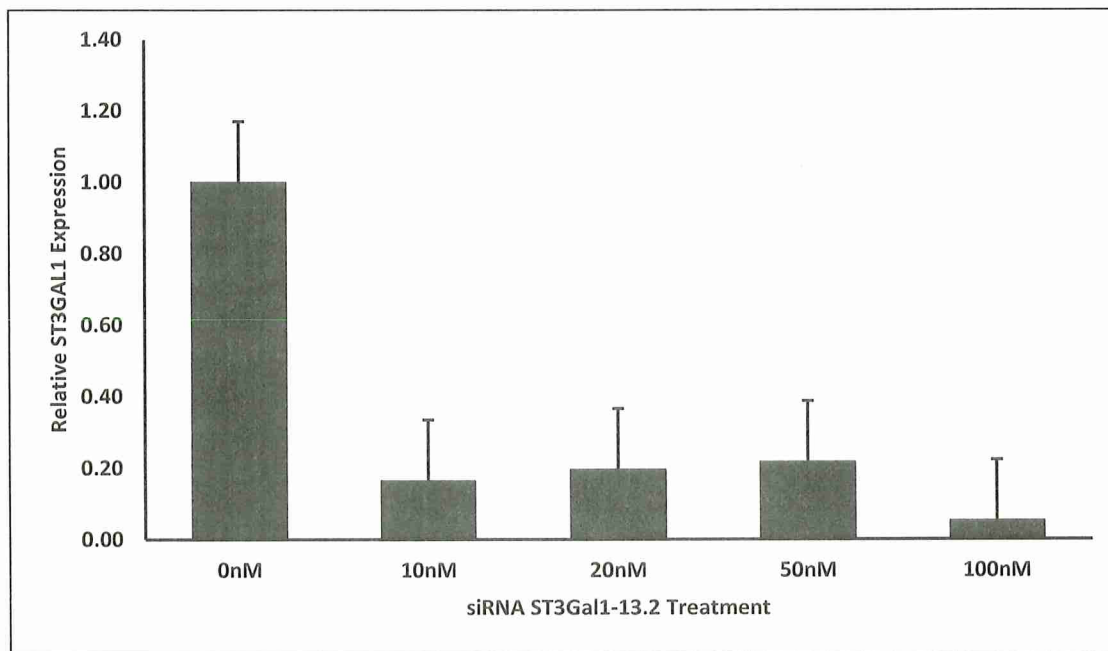


Figure 9. Comparison of siRNA knockdown efficiency. Varying concentrations of siRNA were tested to determine concentration for optimal knockdown of *SIAT4A*, with 100nM providing the highest level of knockdown. Data is representative of three replicates per treatment group.

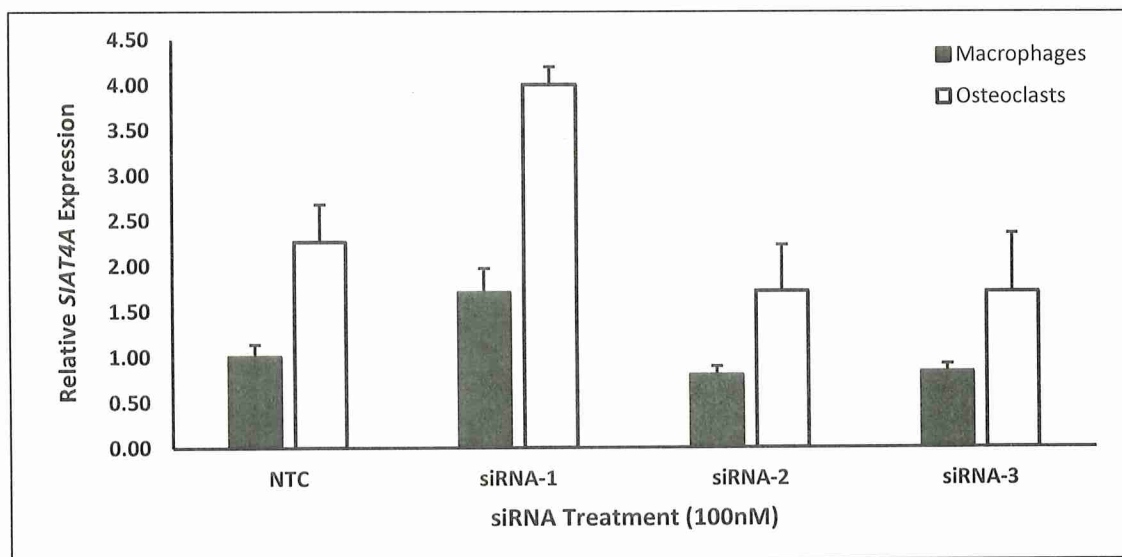


Figure 10. Combined RT-qPCR data from siRNA treatments. Three different siRNA variants targeting different regions of the mature *SIAT4A* transcript were tested for knockdown efficiency in both macrophage precursors and terminally differentiated osteoclasts. Two-tailed, heteroscedastic T-tests did not show any statistically significant differences between the treatment and control groups in the two cell types. Data for macrophages are representative of two experiments with three replicates. Data for osteoclasts are representative of four experiments with three replicates.

After the inconsistency of the results obtained from directly transfecting siRNAs—both in terms of transfection efficiency, and in resultant mRNA levels—we elected to move on to using shRNAs and deliver them using a virus (transduction). While viral transduction efficiency was higher than that of lipofectant-mediated transfection, RT-qPCR results following shRNA-mediated knockdown showed a modest reduction (~65%) in only one of the shRNA variants (Fig. 11).

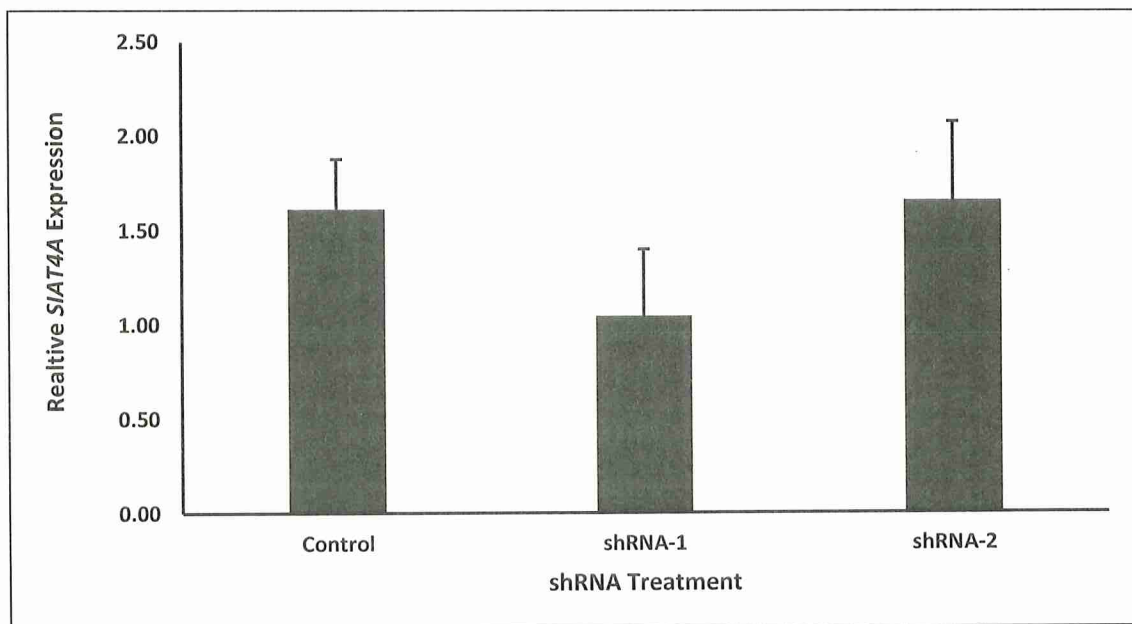


Figure 11. Combined RT-qPCR data from shRNA treatments. Two-tailed, heteroscedastic T-tests did not show any significant difference between any of the treatment groups. Data is representative of two experiments with three replicates per treatment group.

Western and Lectin Blots

To verify that any observed change in *SIAT4A* expression reflected a concomitant change in ST3Gal1 synthesis, we performed a series of western blots for ST3Gal1 itself. Unfortunately, each of the three antibodies that we tried were nonreactive to mouse ST3Gal1—whose reported molecular mass on a reducing SDS-PAGE is 35-45 kDa—as the two sets of bands visible from an early knockout experiment are >80 kDa and >115 kDa, respectively (Fig. 12), and ~75 kDa in a basal expression vs. overexpression experiment (Fig. 13). It is possible these bands represent off-target binding of the antibodies.

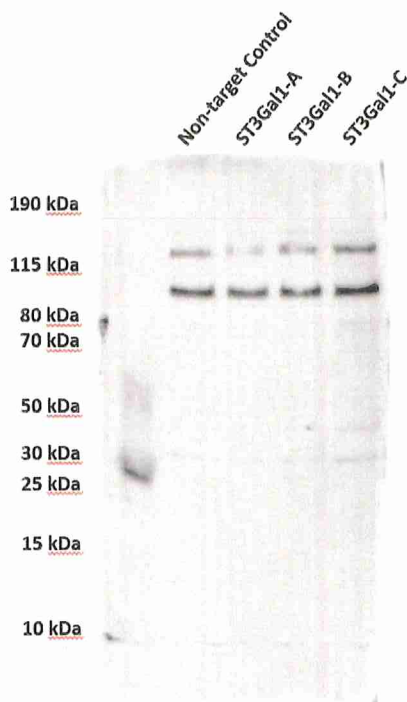


Figure 12. ST3Gal1 Knockout western blot from 3-17-2020.

While there are clearly visible bands, the reported size of ST3Gal1 on an SDS-PAGE under reducing conditions is 35-45 kDa, thus neither set of bands correlates to ST3Gal1. The suffixes -A, -B, and -C indicate the different siRNA variants.

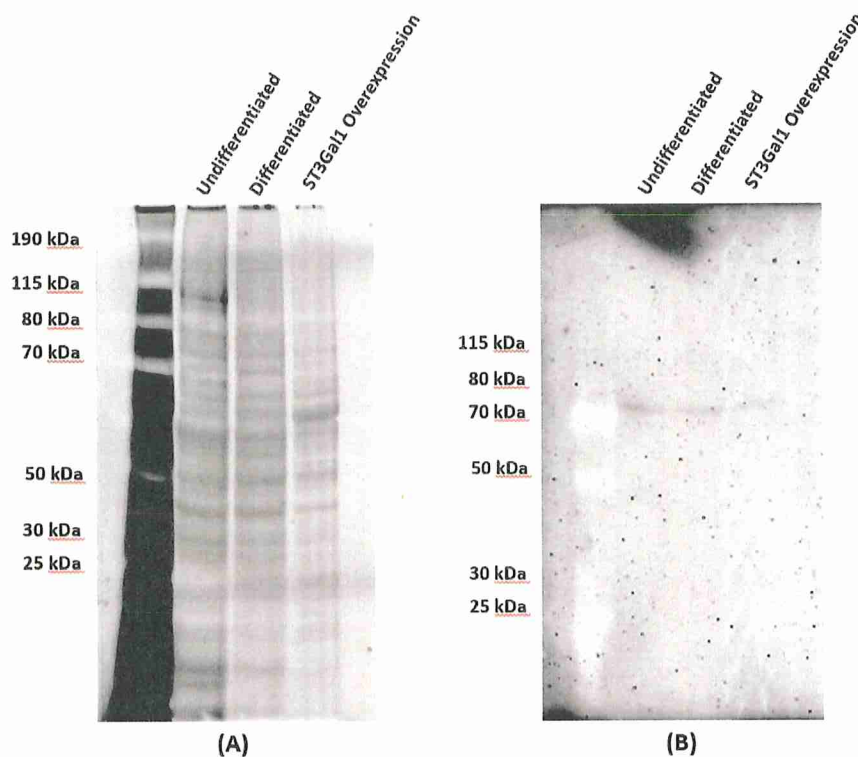


Figure 13. ST3Gal1 basal vs. overexpression total protein stain and western blot. Like Fig. 15, the bands visible in this western blot do not coincide with ST3Gal1, as their apparent molecular weight is too large compared to ST3Gal1's reported weight.

As an alternative means of testing for the presence of ST3Gal1 following knockdown and neuraminidase experiments, we also blotted with lectins for the presence of α 2,3-linked sialic acid on mature osteoclasts and compared the sialylation status to that of neuraminidase-treated osteoclasts. We were able to confirm that treatment with an α 2,3-neuraminidase resulted in a reduction of α 2,3-sialylation (Fig. 14), but treatment with siRNAs did not result in a substantial reduction of ST3Gal1 synthesis, denoted by the lack of a notable decrease in band intensity and densitometry readings (Fig. 15).

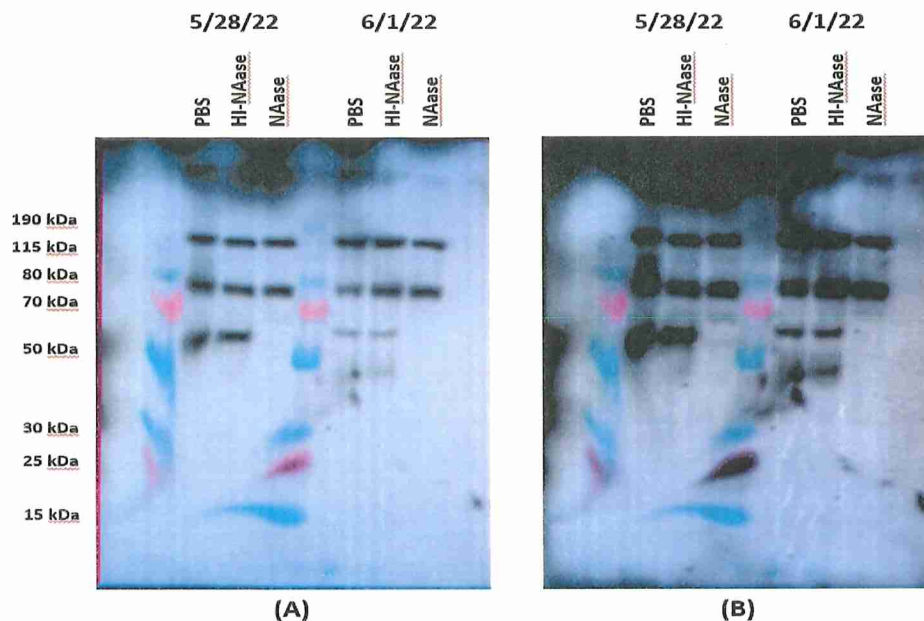


Figure 14. Lectin blot following neuraminidase treatment. PBS treatment was included as a treatment control, whereas heat-inactivated neuraminidase was included to control for any changes that may have arisen from the exogenous nature of the enzyme. (A) 5 min cumulative imaging exposure time. (B) 12 min cumulative imaging exposure time.

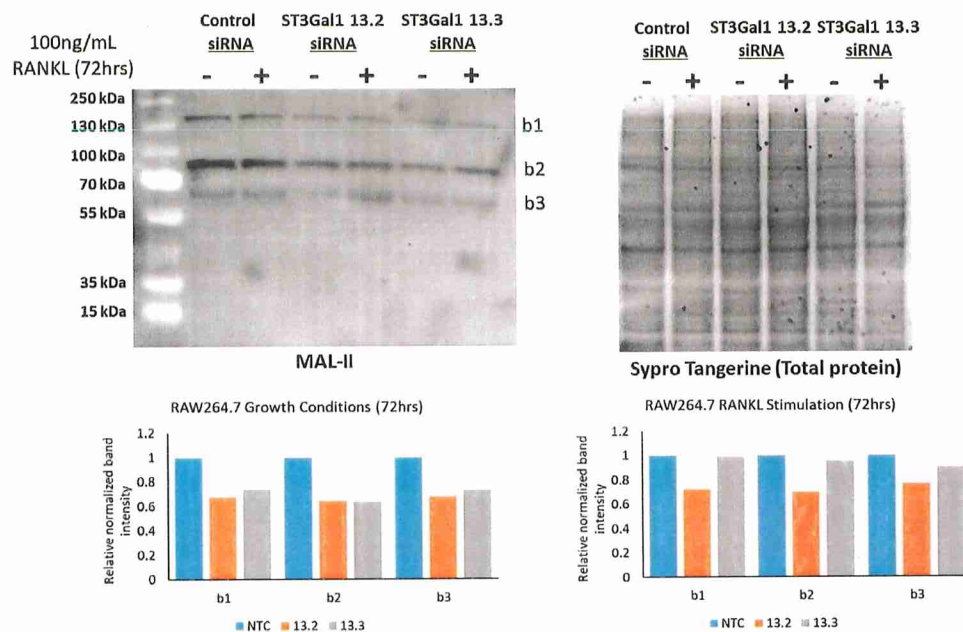


Figure 15. Lectin blot following gene knockdown. siRNA Treatment resulted in only a mild reduction in α 2,3-sialylation, based on densitometry of band intensities.

Neuraminidase Treatments

We recapitulated the neuraminidase experiment that was previously performed on BMMs, instead using RAW 264.7 cells. We did not see an aberrant morphology after treatment, as was seen in the BMMs (Fig. 16).

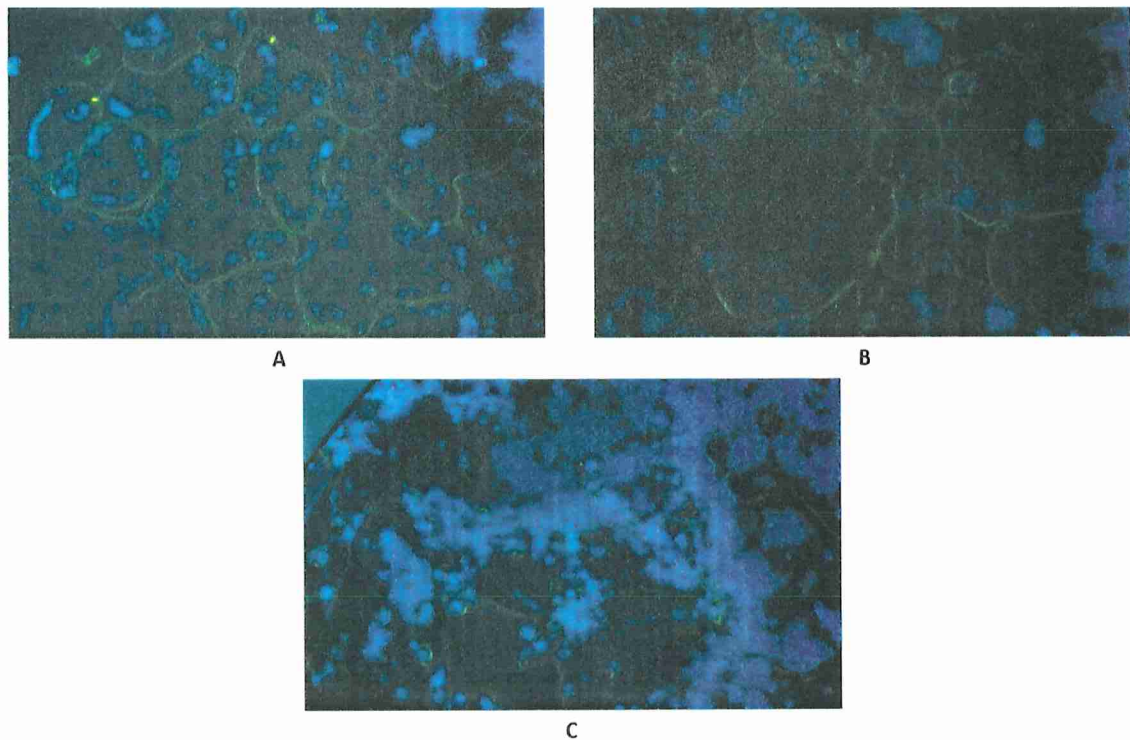


Figure 16. Terminally differentiated osteoclasts derived from RAW 264.7 cells, with or without neuraminidase treatment. (A) PBS, (B) HI-NAase, (C) NAase. Treatments were applied to cells 48hrs after stimulation with RANKL, with differentiation culminating 72hrs after RANKL stimulation. PBS served as the total negative control, whereas heat-inactivated neuraminidase served as the exogenous protein control. Images taken at 4X magnification.

Cell Size – SIAT4A Knockdown vs. Neuraminidase Treatment

Quantified data from shRNA (Fig. 17) and NAase (Fig. 18) treatments did not show a consistent trend in cell size between control groups—Control-1 & -2 in shRNA treatments; PBS in NAase treatments—and treatment groups.

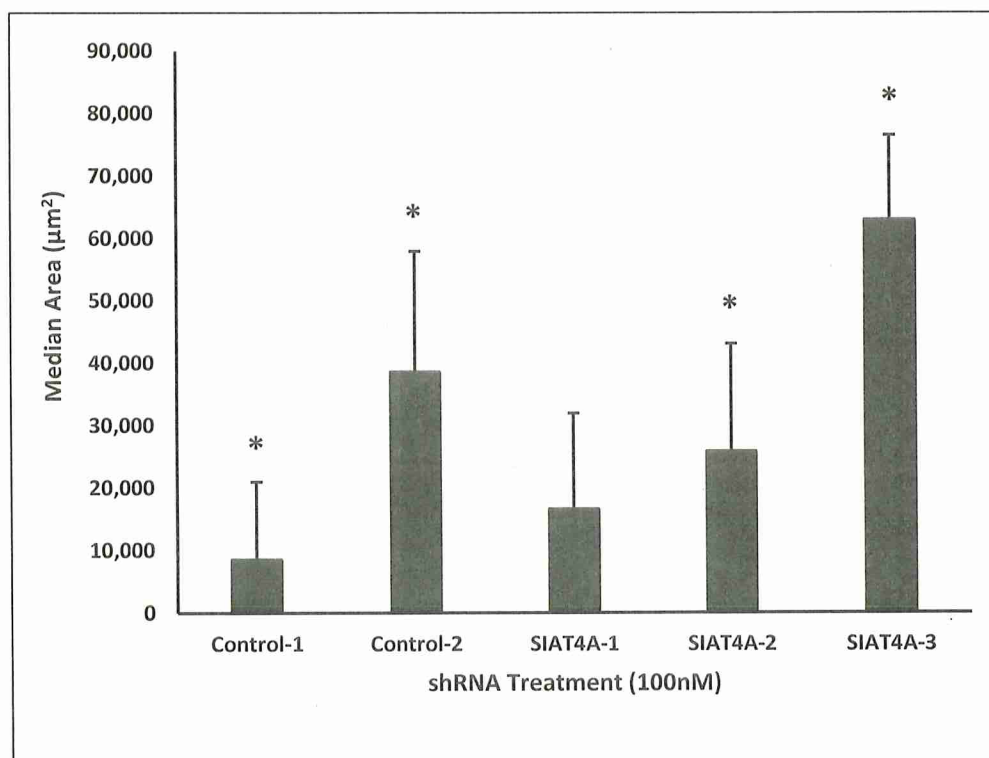


Figure 17. Median cell size following gene knockdown. Data is representative of three experiments with at least three replicates per treatment group. Two-tailed, heteroscedastic T-tests showed significant differences in three groups compared to Control-1. * $p \leq 0.05$.

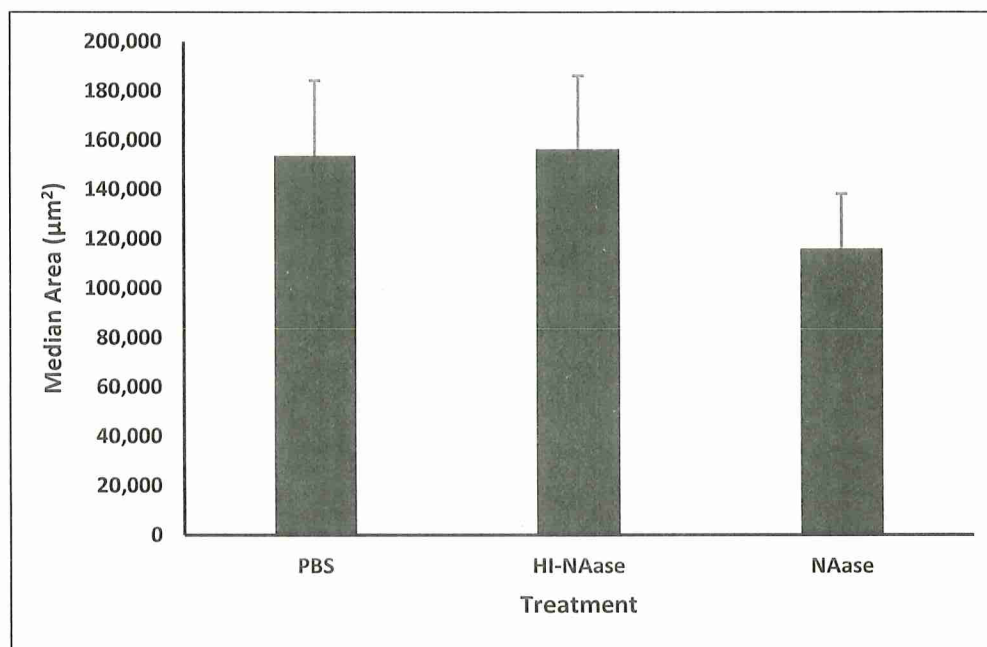


Figure 18. Median cell size following NAase treatment. Data is representative of a single experiment with five replicates per group. Two-tailed, heteroscedastic T-tests did not show any significant differences.

DISCUSSION

Our initial hypothesis—that a reduction in cell-surface α 2,3-linked sialic acid would result in smaller and morphologically aberrant osteoclasts—was not supported. Quantification of cell size following *SIAT4A* knockdown and NAase treatment experiments showed inconsistent results in shRNA-treated cells, and only a mild reduction in NAase-treated cells. Additionally, the variability in results obtained from using RAW 264.7 cells also makes it difficult to obtain statistical significance when comparing data from multiple experiments. The impetus for using RAW 264.7 cells in place of BMMs was twofold: RAW

264.7 cells are easily culturable (with infinite expandability), and they are much cheaper to use long-term compared to primary BMMs—which require the euthanasia of a mouse each time you would perform an experiment. However, these cells displayed a resilience against genetic manipulation, and due to the high propensity for genetic drift in RAW 264.7 cells, determining whether a genetic manipulation was successful also proved more difficult in comparison to other cell types. Another major difference between RAW 264.7 cells and primary macrophages that makes them more desirable for use is that RAW 264.7 cells do not require M-CSF to survive or differentiate, whereas primary cells do. Furthermore, there is evidence that the receptor for M-CSF (c-fms) is sialylated (Rettenmier et al., 1986), and since RAW 264.7 cells do not depend on direct c-fms stimulation, they likely would have a less robust response to desialylation if that is the basis for the morphological change previously seen in primary cells. Unfortunately, the sialylation pattern of c-fms was not established by Rettenmier et al., and further work would need to be done to ascertain whether our particular treatments—which facilitated the removal of α 2,3-linked sialic acid, specifically—would have affected c-fms's sialylation status. Immunoprecipitation of c-fms, followed by treatment with heat-inactivated and functional α 2,3-neuraminidase, individually, and a lectin blot could provide answers to this question. Lastly, repeating the knockdown/knockout experiments in

primary macrophages could be a promising avenue for future experiments.

REFERENCES

- Arai, F., Miyamoto, T., Ohneda, O., Inada, T., Sudo, T., Brasel, K., . . . Suda, T. (1999). Commitment and differentiation of osteoclast precursor cells by the sequential expression of c-Fms and receptor activator of nuclear factor kappaB (RANK) receptors. *J Exp Med*, 190(12), 1741-1754. <https://doi.org/10.1084/jem.190.12.1741>
- Ashley, J. W. (2011). *Significance and Regulation of CD68 Expression in the Osteoclast* [University of Alabama]. Birmingham, Alabama.
- Keever, A. (2019). *Sex-Specific Gene Expression and Its Effect on Osteoclast Maturation* [Eastern Washington University].
- Krueger, U., Bergauer, T., Kaufmann, B., Wolter, I., Pilk, S., Heider-Fabian, M., . . . Konrad, J. (2007). Insights into effective RNAi gained from large-scale siRNA validation screening. *Oligonucleotides*, 17(2), 237-250. <https://doi.org/10.1089/oli.2006.0065>
- Li, N., Sun, J., Benet, Z. L., Wang, Z., Al-Khodor, S., John, S. P., . . . Fraser, I. D. (2015). Development of a cell system for siRNA screening of pathogen responses in human and mouse macrophages. *Sci Rep*, 5, 9559. <https://doi.org/10.1038/srep09559>
- Park, J. H., Lee, N. K., & Lee, S. Y. (2017). Current Understanding of RANK Signaling in Osteoclast Differentiation and Maturation. *Mol Cells*, 40(10), 706-713. <https://doi.org/10.14348/molcells.2017.0225>
- Rettenmier, C. W., Sacca, R., Furman, W. L., Roussel, M. F., Holt, J. T., Nienhuis, A. W., . . . Sherr, C. J. (1986). Expression of the human c-fms proto-oncogene product (colony-stimulating factor-1 receptor) on peripheral blood mononuclear cells and choriocarcinoma cell lines. *J Clin Invest*, 77(6), 1740-1746. <https://doi.org/10.1172/JCI112496>
- Stanley, E. R., & Chitu, V. (2014). CSF-1 receptor signaling in myeloid cells. *Cold Spring Harb Perspect Biol*, 6(6). <https://doi.org/10.1101/cshperspect.a021857>
- Takahata, M., Iwasaki, N., Nakagawa, H., Abe, Y., Watanabe, T., Ito, M., . . . Minami, A. (2007). Sialylation of cell surface glycoconjugates is

essential for osteoclastogenesis. *Bone*, 41(1), 77-86.
<https://doi.org/10.1016/j.bone.2007.03.016>

Takayanagi, H. (2007). Osteoimmunology: shared mechanisms and crosstalk between the immune and bone systems. *Nat Rev Immunol*, 7(4), 292-304. <https://doi.org/10.1038/nri2062>

Teitelbaum, S. L. (2007). Osteoclasts: what do they do and how do they do it? *Am J Pathol*, 170(2), 427-435.
<https://doi.org/10.2353/ajpath.2007.060834>

Wright, N. C., Looker, A. C., Saag, K. G., Curtis, J. R., Delzell, E. S., Randall, S., & Dawson-Hughes, B. (2014). The recent prevalence of osteoporosis and low bone mass in the United States based on bone mineral density at the femoral neck or lumbar spine. *J Bone Miner Res*, 29(11), 2520-2526. <https://doi.org/10.1002/jbmr.2269>

VITA

Author: Christopher S. Harding

Place of Birth: Hamilton, Montana

Undergraduate Schools Attended: Walla Walla Community College
Eastern Washington University

Degrees Awarded: Bachelor of Science in Biology, Eastern Washington
University, 2017

Professional Experience: Tutor, Eastern Washington University, 2019
Teaching Assistant, Eastern Washington
University, 2019-2020